HHS Public Access

Author manuscript

Cerebellum. Author manuscript; available in PMC 2016 December 01.

Published in final edited form as:

Cerebellum. 2015 December ; 14(6): 613–623. doi:10.1007/s12311-015-0652-1.

Tract profiles of the cerebellar white matter pathways in children and adolescents

Yael Leitner[#1], **Katherine E. Travis**[#2], **Michal Ben-Shachar**[3,4], **Kristen W. Yeom**[5], and **Heidi M. Feldman**[2,*]

[1]Child Development Center, Tel Aviv Sourasky Medical Center, Sackler School of Medicine, Tel Aviv University, Tel Aviv, Israel

[2]Department of Pediatrics, Stanford University School of Medicine, Palo Alto CA USA

[3]The Gonda Brain Research Center, Bar Ilan University, Ramat Gan, Israel

[4]The English Department, Linguistics Division, Bar Ilan University, Ramat Gan, Israel

[5]Department of Radiology, Stanford University School of Medicine, Palo Alto CA USA

[#] These authors contributed equally to this work.

Abstract

Intact development of cerebellar connectivity is essential for healthy neuromotor and neurocognitive development. To date, limited knowledge about the microstructural properties of cerebellar peduncles, the major white matter tracts of the cerebellum, is available for children and adolescents. Such information would be useful as a comparison for studies of normal development, clinical conditions, or associations of cerebellar structures with cognitive and motor functions. The goal of the present study was to evaluate the variability in diffusion measures of the cerebellar peduncles within individuals and within a normative sample of healthy children. Participants were 19 healthy children and adolescents, aged 9-17 years, mean age 13.0 +/−2.3. We analyzed diffusion magnetic resonance imaging (dMRI) data with deterministic tractography. We generated tract profiles for each of the cerebellar peduncles by extracting four diffusion properties (fractional anisotropy (FA), mean-, radial-, and axial-diffusivity) at 30 equidistant points along each tract. We were able to identify the middle cerebellar peduncle and the bilateral inferior and superior cerebellar peduncles in all participants. The results showed that within each of the peduncles, the diffusion properties varied along the trajectory of the tracts. However, the tracts showed consistent patterns of variation across individuals; the coefficient of variation for FA across individual profiles was low (≤ 20%) for each tract. We observed no systematic variation of the diffusion properties with age. These cerebellar tract profiles of the cerebellar peduncles can serve as a reference for future studies of children across the age range and for children and adolescents with clinical conditions that affect the cerebellum.

[*]Correspondence Division of Neonatal and Developmental Medicine, Department of Pediatrics Stanford University School of Medicine 750 Welch Road, Suite 315 Palo Alto CA, 94304, USA hfeldman@stanford.edu.

Conflict of Interest Statement: All authors do not report any conflicts of interest.

Keywords

cerebellum; diffusion magnetic resonance imaging (dMRI); white matter; tractography; premature birth; development

Introduction

The cerebellum plays an important role in motor functions, coordination, cognition and emotion (1-4). It is important to understand cerebellar anatomy in children because several disease processes injure or disrupt the cerebellum specifically in children (5, 6). For example, posterior fossa brain tumors account for a high proportion of pediatric brain tumors (7, 8). Abnormal cerebellar development is a complication of extreme prematurity (9-11) and has been associated with poor developmental outcomes (12). Cerebellar injury or dysmaturity has been implicated in developmental disabilities, such as autism (13). Studies to date of cerebellar anatomy in children and adolescents tend to evaluate the size or volume of the entire cerebellum (14-16), selected compartments (14), or lobular structures (17). Few studies in children and adolescents have evaluated cerebellar white matter tracts (18). The present study examined the structural characteristics of the three major pathways of the cerebellar peduncles in a healthy pediatric sample. Examining structural properties of the peduncles in children has important theoretical implications for understanding the pathways of neural signals in motor, cognitive, and emotional processes (19, 20). Quantifying individual differences in healthy and typically developing children is a necessary prerequisite to understanding variations in clinical conditions that affect the cerebellum.

The three major white matter pathways of the cerebellar peduncles link the cerebellum to the cerebral hemispheres and to the spinal column. The right and left inferior cerebellar peduncles (ICP) are a major afferent pathway, feeding signals from the spine and the olivary nucleus into the cerebellum. The ICP also contains efferent connections from the cerebellum towards the vestibular nuclei along the border of the pons and medulla (21). The middle cerebellar peduncle (MCP), the largest of the structures, is a prominent tract with a “horse shoe” appearance. It is a major afferent pathway that carries input fibers from the contralateral cerebral cortex via pontine nuclei across the midline of the cerebellum to the cerebellar cortex. In anatomical cross-sections, fibers comprising the MCP can be observed to diverge around the pontine nuclei (21). The right and left superior cerebellar peduncles (SCP) are primarily cerebellar efferent pathways. The SCP emerges from the deep cerebellar nuclei, including the dentate of the cerebellum, and travels through the ipsilateral superior cerebellar peduncle into the dorsal pons, decussates at the level of the inferior colliculus, and travels to the contralateral cerebral cortex via the thalamus.

Diffusion magnetic resonance imaging (dMRI) can be used to visualize and characterize the white matter microstructure. Pathways of the cerebellum have been described within healthy adults (22) and adults with clinical conditions including ataxia (23), degenerative spinocerebellar disease (24) and schizophrenia (25). Diffusion MRI has documented reductions in fiber tract volume and signal intensities at the level of the superior cerebellar peduncle and midline cerebellar structures after posterior fossa tumor treatments (26). The

predominant dMRI measure used to index white matter microstructure is fractional anisotropy (FA), a scalar value that indexes the degree of directional preference in the pattern of water diffusion (27, 28). It can be decomposed into axial diffusivity (AD) and radial diffusivity (RD), measures for the speed of water diffusion along the principal and perpendicular diffusion directions, respectively. Mean diffusivity (MD) assesses the overall rate of water diffusion across the three principal axes. Mean tract FA of the cerebellar tracts have been found to correlate with the severity of cerebral palsy in children born preterm with and without periventricular leukomalacia (29) and with motor functioning in children with autism spectrum disorders (30).

Quantifying diffusion measures along the trajectories of fiber bundles has been proven extremely useful in the analysis of cerebral pathways (31-33). Such methods generate tract profiles, vectors of diffusion properties along the trajectory of white matter tracts. The tract profiles provide a high degree of specificity about the underlying tissue properties that cannot otherwise be distinguished with mean tract measures. In addition, tract profiles can be used to compare the white matter characteristics of a single subject to standardized tract profiles from a healthy sample to elucidate characteristics of the individual (31). Reliable identification of cerebellar white matter tract profiles may improve prediction of abnormal outcomes of various health conditions, particularly in conditions that have minimal findings on conventional studies, and may prove clinically relevant to guide surgical interventions that avoid unnecessary injury, particularly in resections of cerebellar tumors.

This study characterizes the microstructure of the major white matter tracts of the cerebellum in a sample of healthy children and adolescents using dMRI, deterministic tractography, and an analytic strategy that generates tract profiles. The first goal was to assess the variability in FA and other diffusion properties (MD, RD, and AD) along the extent of each cerebellar peduncle within individuals. The second goal was to establish the variability of tract profiles across individuals and specifically to assess whether the diffusion properties would vary systematically as a function of age. Based on the use of similar methods to characterize cerebral tracts (31), we predicted that diffusion properties would vary along the trajectory of each of the cerebellar peduncles and that profiles would be similar across individuals. We further predicted that the diffusion properties would not differ on the basis of age given evidence demonstrating rapid cerebellar white matter maturation in the first 3 years of life (18).

Materials and methods

Subjects

This healthy normative sample was comprised of 19 children and adolescents, aged 9-17 years, 9 of whom were male, with a mean age of 13.0 +/− 2.3 years. The participants represented the entire sample of healthy children who enrolled in the Palo Alto, CA site of a multi-site larger imaging study (34, 35) with the exception of one child from that sample was excluded because of an incidental finding of a subarachnoid cyst. All of the participants were free of neurological, learning, behavioral, or emotional disorders because such conditions may be associated with altered brain structure. The Stanford University institutional review board approved this study and consent procedures. A parent or legal

guardian provided informed written consent and children provided written assent. Participants were compensated for participation.

MRI acquisition and processing

MRI data were acquired on a 3T Signa Excite (GE Medical Systems, Milwaukee, WI) at Stanford University. T1 images included one high resolution inversion recovery (IR)-prep 3D fast spoiled gradient (FSPGR) scan collected in the axial plane and a second set of T1 images were co-registered to the first FSPGR using a mutual information maximization algorithm (SPM5, http://www.fil.ion.ucl.ac.uk/spm/). Review of T1 scans by an experienced pediatric neuroradiologist (KWY) confirmed that all participants had no cortical or cerebellar abnormalities on the T1-weighted images.

For dMRI and tractography, a diffusion-weighted, single-shot, spin-echo, echo-planar imaging sequence (TE = 80 ms, TR = 6700 ms, FOV = 24 cm, matrix size = 128 × 128) was used to acquire 60 slices, 2 mm thick, in 30 different diffusion directions (b = 900). The sequence was repeated 4 times, and 10 non-diffusion weighted (b = 0) volumes were collected. Total diffusion scan time with 4 repetitions lasted approximately 14.5 minutes. Total scan time for all diffusion and structural scans was approximately 30 minutes.

dMRI images were pre-processed with open-source software, mrDiffusion (http://white.stanford.edu/software/). Eddy current distortions and subject motion in the diffusion weighted images were removed by a 14-parameter constrained non-linear co-registration algorithm based on the expected pattern of eddy current distortions, given the phase-encoding direction of the acquired data (36). Diffusion tensors were fit using a robust least-squares algorithm designed to remove outliers at the tensor estimation step (37). We computed the eigenvalue decomposition of the diffusion tensor and the resulting eigenvalues were used to compute the fractional anisotropy (FA), mean diffusivity (MD), radial diffusivity (RD) and axial diffusivity (AD) of each voxel in the diffusion MR images (38).

Fiber tract identification

dMRI fiber tractography and tract quantification were performed using mrDiffusion. For each white matter cerebellar tract, tracking was initiated by seeding a manually placed region of interest (ROI) on the principal diffusion direction map (red-green-blue (RGB) map). Spherically shaped ROIs, 5 mm in diameter, were placed by a child-neurologist (YL) based on annotated RGB maps in a diffusion MRI atlas (39)(see below for a detailed description). This procedure is comparable to ROI placement methods previously used to identify the ICP, MCP, and SCP in adults (22). A pediatric neuroradiologist (KWY) confirmed proper ROI placement in each subject. Only minimal changes were necessary because the ROI placement was in close agreement for all tracts. Fibers were tracked from 8 seed points per voxel within the ROIs using a deterministic streamlines tracking algorithm (37, 40, 41) with a fourth-order Runge-Kutta path integration method (42). For tracking purposes, a continuous tensor field was estimated using trilinear interpolation of the tensor elements. Tracking proceeded in all directions at a step size of 1mm; tracking was stopped when FA dropped below a minimum threshold of .15 or when the angle between two adjacent steps was greater than 30°. These tracking parameters are comparable to those used

to identify both cerebral and cerebellar tracts in adults (43). We chose a restrictive angle because of the high proportion of crossing fibers within the cerebellum (44, 45). Each fiber group was then restricted by a second manually placed ROI (Figure 1) in order to constrain the detected tracts according to established neuroanatomical knowledge of the cerebellar peduncles. The fiber tract trajectory was verified and tracts were cleaned of any anatomically incompatible streamlines (e.g., pontine crossing fibers, fibers that cross through the corpus callosum, fibers between cortex and cerebellum not crossing the midline at the level of the pons or thalamus). Tract editing was performed manually and individually using a 3D visualization tool (QUENCH, http://white.stanford.edu/newlm/index.php/QUENCH) guided by a neuroanatomy atlas (39) and by published cerebellar tracking results in adults (22, 44).

ROI placement

Inferior Cerebellar Peduncle tracts, Right and Left (ICP)—The first spherical ROI was placed on the ICP (blue voxels on the red-green-blue map) defined on the axial plane at the level of the medulla, inferior to the dentate nucleus (Figure 1a). The second spherical ROI was placed on the ipsilateral ICP (green voxels on the RGB map) defined on the axial plane at the level of the ponto-mesencephalic junction, as described by Mori et al. 2005 (39) (Figure 1b). Fibers were tracked from ROI1, and the resulting fiber group was intersected with ROI2 to keep only streamlines passing through both ROIs (Figure 1c). The trajectory of the ICP matched the configuration described by other researchers (22).

Middle Cerebellar Peduncle Tract (MCP)—The MCP was consistently identified on the axial red-green-blue (RGB) map at the level of the medial pons, in the most caudal slice in which the dentate nucleus was visible (Figure 1d). Pontine fibers of the MCP first exit the pontine nuclei and decussate across the midline (red on RGB map) before entering the cerebellum, where fibers are predominantly oriented in the anterior-posterior direction (green on RGB map). The MCP was captured by placing two spherical ROIs in central portions of the right and left MCP within the cerebellum, (39) (Figure 1d). Tracking was initiated from the left ROI. The resulting streamlines were intersected (via an “AND” operation) with the right ROI to include only those streamlines passing through both ROIs. This approach produces streamlines that bifurcate into two separate branches (39), reflecting the passage of ponto-cerebellar fibers around the pontine nuclei (21). Since calculations of tract profiles are assumed to be coherent and non-branching, streamlines passing posterior to the pontine nuclei as the pontine crossing tract, were removed manually using QUENCH for each subject (Figure 1e) (31). One subject was excluded from quantitative analyses of the MCP because only the pontine crossing tract could be identified for this participant.

Superior Cerebellar Peduncle tracts, Left and Right (SCP)—One spherical ROI was placed on the dentate nucleus in the axial plane of the RGB map at the level of the medial pons (Figure 1f). The second spherical ROI was placed on the ipsilateral superior cerebellar peduncle, (green voxels on the RGB map) at the level of the decussation of the superior cerebellar peduncles, at the ponto-mesencephalic junction (Figure 1g). Using deterministic tracking methods, we could not follow this tract dorsally through the decussation towards the contralateral cortex, but rather identified fibers continuing on the

ipsilateral side to the cortex, as described by Mori et al. (39). We therefore clipped the tract at the level of the decussation, and analyzed its diffusivity properties below that point (Figure 1h).

Fiber tract quantification

For each cerebellar peduncle, we used the two waypoint ROIs (described above) to restrict the central portion of the tract. The central portion bounded by the two ROIs is generally consistent across individuals, whereas the extreme ends of a fascicle typically vary across subjects and are more likely to be affected by partial volume-averaging with adjacent gray matter. Therefore, diffusion properties of each cerebellar peduncle were quantified along this central portion of the tract (Figure 1) by resampling each tract to 30 equidistant nodes. Diffusion measurements (fractional anisotropy (FA), mean diffusivity (MD), radial diffusivity (RD), and axial diffusivity (AD)) were calculated at each node of each fiber using a spline interpolation of the diffusion properties. Diffusion measures are summarized at each node by taking a weighted average of the diffusion measure at that node on each fiber. Each fiber's contribution to the average was weighted by the probability that a fiber was a member of the fascicle, computed as the Mahalanobis distance from the fiber tract core (31). This procedure minimizes the contribution of fibers located further from the fiber tract core that are more likely to reflect a mixture of gray and white matter, and so minimizes the effect of partial volume-averaging on diffusion property estimates. This approach is particularly important in quantifying the relatively thin cerebellar pathways that pass adjacent to gray matter.

Statistical Analyses

Tract profiles were generated using open source software (https://github.com/jyeatman/AFQ.git) integrated within mrDiffusion (white.stanford.edu/software/). Tract profiles were created by calculating the mean and standard deviation of each diffusion property (e.g., FA, MD, RD, AD) at each node (30 total) of the tract. To assess the consistency of individual tract profiles, we performed a one-way repeated measures ANOVA, using 3 tract locations as the within subject independent variable and mean FA as the dependent variable. Individual subjects served as a fixed factor in this model. The three locations of each tract corresponded to the average FA in nodes 1-10, 11-20 and 21-30. We reasoned that if FA varied consistently and significantly along the tract then we would expect a main effect of Location on FA. We also used the means and standard deviations from this study to calculate the coefficient of variation (CV) for each location to assess the relative amount of individual variability for each tract. The coefficient of variation is calculated as the mean divided by the standard deviation. We compared these calculated CV values of FA to comparable CV values that we computed using mean FA and standard deviation measures from previously reported data for the ICP, MCP and SCP within study of younger typically developing neonates and children (18). We did not calculate CV for AD and RD because these diffusion properties comprise FA and thus the assessments would not be independent.

To assess whether FA along the trajectory of each tract varied by age, we first calculated Spearman correlation coefficients between age and FA along the tract profile. To achieve greater power, we also performed independent Student's t-tests along the average FA tract

profile of younger (ages 9-13 years; mean age = 11.2 years; n = 10) as compared to older children (13-17; mean age = 14.8 years; n = 9) based on a median split of the sample. A family-wise error corrected cluster size was computed using a nonparametric permutation method to correct for multiple comparisons (46).

Results

We successfully identified the inferior, middle, and superior cerebellar peduncles in all participants in the normative group. Figure 2 shows the cerebellar pathways for a representative subject. In one subject, the MCP was limited to ponto-cerebellar fibers comprising the pontine crossing tract. For this reason, the data from this individual were not included in the group analysis of the MCP.

FA tract profiles for the ICP, MCP and SCP are presented in Figures 3 and 4. Systematic variations in FA are seen along the trajectory of each tract. In both left and right ICP, FA initially increases, corresponding to the narrowing of the tract as it enters the cerebellum, followed by a more gradual decrease within the cerebellum, possibly related to intracerebellar crossing fibers (Figure 3a, b). Conversely, in the MCP, FA decreases as the tract passes medially through the pontine nuclei (Figure 3c). In both left and right SCP, FA increases gradually as the tracts exit the cerebellum and enter the brainstem (Figure 4a,b). In both the ICP and MCP, reductions in FA are associated with increasing MD and RD but no change in AD (Figure 5). In the ICP, increased FA is primarily associated with increased MD and AD, with only minimal change in RD (Figure 5).

Repeated-measures ANOVA analyses calculated for each tract confirmed that FA differed significantly between the tract segments in each tract in a highly consistent manner: left inferior cerebellar peduncle $F(2, 36) = 12.5$ $p < 0.001$, right inferior cerebellar peduncle $F(2,36) = 13.9$ $p < 0.001$, middle cerebellar peduncle $F(2, 34) = 38.4$ $p < 0.001$, left superior cerebellar peduncle $F(2,36) = 61.3$ $p < 0.001$ and right superior cerebellar peduncle $F(2,36) = 23.1$ $p < 0.001$. These analyses demonstrate that FA changes significantly along the trajectory of the each of the separate cerebellar tracts. A visual presentation of the repeated measures analysis is shown in Figure 6; variations in the mean FA for the 3 locations demonstrates that FA changes along the trajectory of the each of the tracts; the standard deviations demonstrate that inter-individual variation is minimal.

For all tracts, the CV of FA was calculated to be < 20% (Table 1). This degree of relative individual variability appears consistent with CV values that we calculated based on the mean FA and standard deviation values of the ICP, MCP and SCP reported in a previous study of younger children (18). In that study, CV values for FA were as follows: ICP 17.6%, MCP 13.3%, SCP 17.1% (left and right not differentiated).

FA did not correlate significantly with age for any of the five cerebellar tracts ($p > 0.05$ for all tracts). We found no significant group differences in FA values between the younger and older age groups for any location along the trajectory of each cerebellar tract ($p > 0.05$).

Discussion

We identified the cerebellar peduncles using dMRI and tractography in a normative sample of healthy, typically developing children and adolescents. We generated tract profiles for each of the cerebellar peduncles by calculating four diffusion properties (FA, MD, RD, and AD) at 30 equidistant points along the tracts. We found significant and consistent variations in the four diffusion parameters along the trajectory of each of the five cerebellar peduncles. The patterns of variation were highly consistent across the sample. Age was not associated with differences in tract profiles. These results can provide important baseline information for future studies of the development of the cerebellum in healthy children and in clinical pediatric populations.

In all of the healthy children and adolescents in this sample, dMRI and tractography were capable of identifying and characterizing the cerebellar tracts. The observed variations in FA along tract trajectories are highly consistent with established patterns in adults (22). We interpret variations in diffusion properties along tract trajectories as likely related to underlying neuroanatomical features, including restriction in anatomical space and the presence of kissing and crossing fibers (31). This explanation of the variations is supported by the observation that MD, RD and AD differentially contributed to changes in FA in the ICP, MCP and SCP. Follow-up studies would be able to explore the contribution of crossing fibers to diffusion properties of cerebellar pathways through the use of complex diffusion models (47, 48). In addition, future studies can correlate FA or other diffusion properties of the peduncles with motor, cognitive or emotional functions in which the cerebellum has been implicated (1, 2, 4, 6, 49).

We found that individual variation in tract profiles was minimal. The degree of relative individual variability in FA appears consistent with CV values that we derived from mean FA values reported by Saksena and colleagues (18) for the ICP, MCP, and SCP. Moreover, the FA values we found were similar to those reported by Saksena and colleagues (18) with the exception of the ICP, where the FA in our study was higher. We attribute the differences in FA to differences in methodology. Saksena and colleagues (18) used a one ROI method to generate diffusion properties, whereas we used a two-ROI method to generate a tract and calculated the CV from 30 points along the tract.

In our sample, FA within each of the five cerebellar tracts was not significantly associated with age in the normative group. Rapid development of cerebellar white matter occurs within the first three years of life (18) and then slows. This developmental pattern may account for the lack of significant age-associations in children 9 to 17 years of age. However, we recognize that in a small sample age differences may not achieve statistical significance.

One limitation of the study is that the sample size is modest and the age range large. However, the consistency of the tract profiles across individuals within this age range is encouraging that larger studies will find similar patterns. Another limitation of the study is that the methods did not resolve crossing fibers. Given the acquisition parameters including the b-value and number of diffusion gradients applied, we were not able to use methods to

identify intravoxel fiber crossing. However, given that the cerebellum has many intersecting fibers, alternative methods of diffusion data collection should be used for analyzing the cerebellar peduncles (50, 51). A minor limitation is that we did not calculate inter-rater reliability on the placement of the ROIs, but rather used two observers who came to consensus.

In summary, we identified variations of diffusion properties within each of the cerebellar peduncles but similar profiles for each of the peduncles across healthy children and adolescents. We think that the methods described may prove useful for other studies of cerebellar structure and function. The methods we used quantified the diffusion properties along the trajectory of the fiber tracts, creating tract profiles or vectors of the diffusion properties. These tract profiles can be used to compare the white matter characteristics of a single subject to standardized tract profiles from healthy samples to elucidate characteristics of the individual (31). At each point along the tract, the white matter diffusion measure, such as FA can be assigned a percentile or z-score based on the individual's distance from the samples median or mean. The method can locate regions within the cerebellar peduncles, where the individual falls outside the range of normal for the sample or where functions correlate with white matter microstructure. Though it is difficult to compare absolute FA values across scanners and different protocols, the z-score of individuals from the clinical population in relation to a normative sample from the same scanner may be comparable across study sites. These methods may prove useful for documenting subtle cerebellar abnormalities in clinical conditions in which conventional neuroimaging or mean values of diffusion properties may not reveal any differences from normal. These methods may also increase the ability to detect correlations between cerebellar white matter anatomy and functional capabilities. Such methods have been used in adults to identify white matter differences in individuals with Asperger syndrome (52) and temporal lobe epilepsy (53). We have found statistically significant associations of cerebellar white matter properties and reading skills (54). Future studies should replicate the anatomical findings in larger cohorts at various ages to document developmental change. Then these methods can be used to characterize clinical populations and to evaluate cerebellar white matter structure in relation to functions attributed to the cerebellum.

Acknowledgements

This work has been supported in part by the National Institutes of Health, NICHD grants (RO1-HD69162, RO1-HD46500) and the Clinical and Translational Science Award 1UL1 RR025744 for the Stanford Center for Clinical and Translational Education and Research (Spectrum) from the National Center for Research Resources, National Institutes of Health.

This work was also supported by a grant to Dr. Leitner from the Feldman Family Foundation. We thank the children and families who participated in our study; Jason D. Yeatman, Robert Dougherty, and Brian Wandell for helpful suggestions regarding the analyses; and the developmental-behavioral pediatrics research group for discussions of the results and interpretations.

References

1. Ito M. Control of mental activities by internal models in the cerebellum. Nature Reviews Neuroscience. 2008; 9(4):304–13. PubMed PMID: 18319727. [PubMed: 18319727]

2. Hyam JA, Owen SL, Kringelbach ML, Jenkinson N, Stein JF, Green AL, et al. Contrasting connectivity of the ventralis intermedius and ventralis oralis posterior nuclei of the motor thalamus demonstrated by probabilistic tractography. Neurosurgery. 2012; 70(1):162–9. discussion 9. PubMed PMID: 22158304. [PubMed: 22158304]

3. Schmahmann JD. An emerging concept. The cerebellar contribution to higher function. Archives of Neurology. 1991; 48(11):1178–87. PubMed PMID: 1953406. [PubMed: 1953406]

4. Schmahmann JD, Sherman JC. The cerebellar cognitive affective syndrome. Brain. 1998; 121(Pt 4): 561–79. PubMed PMID: 9577385. [PubMed: 9577385]

5. Schmahmann JD. Disorders of the cerebellum: ataxia, dysmetria of thought, and the cerebellar cognitive affective syndrome. Journal of Neuropsychiatry & Clinical Neurosciences. 2004; 16(3): 367–78. PubMed PMID: 15377747. [PubMed: 15377747]

6. Tavano A, Grasso R, Gagliardi C, Triulzi F, Bresolin N, Fabbro F, et al. Disorders of cognitive and affective development in cerebellar malformations. Brain. 2007; 130(Pt 10):2646–60. PubMed PMID: 17872929. [PubMed: 17872929]

7. Central Brain Tumor Registry of the United States (CBTRUS). CBTRUS Statistical Report: Primary Brain and Central Nervous System Tumors Diagnosed in th United States in 2004-2006. Central Brain Tumor Registry of the United States; Hinsdale, IL: 2010. website: http://www.cbtrus.org

8. Arora RS, Alston RD, Eden TO, Estlin EJ, Moran A, Birch JM. Age-incidence patterns of primary CNS tumors in children, adolescents, and adults in England. Neuro-Oncology. 2009; 11(4):403–13. PubMed PMID: 19033157. Pubmed Central PMCID: PMC2743220. [PubMed: 19033157]

9. Limperopoulos C, Soul JS, Gauvreau K, Huppi PS, Warfield SK, Bassan H, et al. Late gestation cerebellar growth is rapid and impeded by premature birth. Pediatrics. 2005; 115(3):688–95. PubMed PMID: 15741373. [PubMed: 15741373]

10. Messerschmidt A, Prayer D, Brugger PC, Boltshauser E, Zoder G, Sterniste W, et al. Preterm birth and disruptive cerebellar development: assessment of perinatal risk factors. European. Journal of Paediatric Neurology. 2008; 12(6):455–60. PubMed PMID: 18222715.

11. Volpe JJ. Brain injury in premature infants: a complex amalgam of destructive and developmental disturbances. Lancet Neurology. 2009; 8(1):110–24. PubMed PMID: 19081519. Pubmed Central PMCID: NIHMS90036 PMC2707149. [PubMed: 19081519]

12. Messerschmidt A, Fuiko R, Prayer D, Brugger PC, Boltshauser E, Zoder G, et al. Disrupted cerebellar development in preterm infants is associated with impaired neurodevelopmental outcome. European Journal of Pediatrics. 2008; 167(10):1141–7. PubMed PMID: 18172680. [PubMed: 18172680]

13. Fatemi SH, Aldinger KA, Ashwood P, Bauman ML, Blaha CD, Blatt GJ, et al. Consensus paper: pathological role of the cerebellum in autism. Cerebellum. 2012; 11(3):777–807. PubMed PMID: 22370873. [PubMed: 22370873]

14. Limperopoulos C, Soul JS, Haidar H, Huppi PS, Bassan H, Warfield SK, et al. Impaired trophic interactions between the cerebellum and the cerebrum among preterm infants. Pediatrics. 2005; 116(4):844–50. PubMed PMID: 16199692. [PubMed: 16199692]

15. Messerschmidt A, Brugger PC, Boltshauser E, Zoder G, Sterniste W, Birnbacher R, et al. Disruption of cerebellar development: potential complication of extreme prematurity. Ajnr: American Journal of Neuroradiology. 2005; 26(7):1659–67. PubMed PMID: 16091510. [PubMed: 16091510]

16. Nopoulos PC, Conrad AL, Bell EF, Strauss RG, Widness JA, Magnotta VA, et al. Long-term outcome of brain structure in premature infants: effects of liberal vs restricted red blood cell transfusions. Archives of Pediatrics & Adolescent Medicine. 2011; 165(5):443–50. PubMed PMID: 21199970. [PubMed: 21199970]

17. Diedrichsen J, Balsters JH, Flavell J, Cussans E, Ramnani N. A probabilistic MR atlas of the human cerebellum. Neuroimage. 2009; 46(1):39–46. PubMed PMID: 19457380. [PubMed: 19457380]

18. Saksena S, Husain N, Malik GK, Trivedi R, Sarma M, Rathore RS, et al. Comparative evaluation of the cerebral and cerebellar white matter development in pediatric age group using quantitative diffusion tensor imaging. Cerebellum. 2008; 7(3):392–400. PubMed PMID: 18581196. [PubMed: 18581196]

19. Limperopoulos C, Chilingaryan G, Guizard N, Robertson RL, Du Plessis AJ. Cerebellar injury in the premature infant is associated with impaired growth of specific cerebral regions. Pediatric Research. 2010; 68(2):145–50. PubMed PMID: 20389260. [PubMed: 20389260]

20. Tam EW, Ferriero DM, Xu D, Berman JI, Vigneron DB, Barkovich AJ, et al. Cerebellar development in the preterm neonate: effect of supratentorial brain injury. Pediatric Research. 2009; 66(1):102–6. PubMed PMID: 19287350. Pubmed Central PMCID: NIHMS107798 PMC2700193. [PubMed: 19287350]

21. Naidich, T.; Duvernoy, H.; Delman, B.; Sorenson, A.; Kollias, S.; Haacke, E. Duvernoy's Atlas of the Human Brain Stem and Cerebellum: High-Field MRI, Surface Anatomy, Internal Structure, Vascularization and 3 D Sectional Anatomy. Springer; Vienna: 2009. p. 876

22. Stieltjes B, Kaufmann WE, van Zijl PC, Fredericksen K, Pearlson GD, Solaiyappan M, et al. Diffusion tensor imaging and axonal tracking in the human brainstem. Neuroimage. 2001; 14(3): 723–35. PubMed PMID: 11506544. [PubMed: 11506544]

23. Hong JH, Kim OL, Kim SH, Lee MY, Jang SH. Cerebellar peduncle injury in patients with ataxia following diffuse axonal injury. Brain Research Bulletin. 2009; 80(1-2):30–5. PubMed PMID: 19505539. [PubMed: 19505539]

24. Taoka T, Kin T, Nakagawa H, Hirano M, Sakamoto M, Wada T, et al. Diffusivity and diffusion anisotropy of cerebellar peduncles in cases of spinocerebellar degenerative disease. Neuroimage. 2007; 37(2):387–93. PubMed PMID: 17583535. [PubMed: 17583535]

25. Kanaan RA, Allin M, Picchioni M, Barker GJ, Daly E, Shergill SS, et al. Gender differences in white matter microstructure. PLoS ONE [Electronic Resource]. 2012; 7(6):e38272. PubMed PMID: 22701619. Pubmed Central PMCID: PMC3368921.

26. Soelva V, Hernáiz Driever P, Abbushi A, Rueckriegel S, Bruhn H, Eisner W, et al. Fronto-cerebellar fiber tractography in pediatric patients following posterior fossa tumor surgery. Childs Nerv Syst. Apr 01; 2013 29(4):597–607. 2013. English. [PubMed: 23184224]

27. Beaulieu C. The Basis of Anisotropic Water Diffusion in the Nervous System - a Technical Review. NMR Biomed. 2002; 15:435–55. [PubMed: 12489094]

28. Feldman HM, Yeatman JD, Lee ES, Barde LH, Gaman-Bean S. Diffusion tensor imaging: a review for pediatric researchers and clinicians. Journal of Developmental & Behavioral Pediatrics. 2010; 31(4):346–56. PubMed PMID: 20453582. [PubMed: 20453582]

29. Wang S, Fan G, Xu K, Wang C. Potential of diffusion tensor MR imaging in the assessment of cognitive impairments in children with periventricular leukomalacia born preterm. European Journal of Radiology. 2013; 82(1):158–64. PubMed PMID: 23084875. [PubMed: 23084875]

30. Hanaie R, Mohri I, Kagitani-Shimono K, Tachibana M, Azuma J, Matsuzaki J, et al. Altered microstructural connectivity of the superior cerebellar peduncle is related to motor dysfunction in children with autistic spectrum disorders. Cerebellum. 2013; 12(5):645–56. PubMed PMID: 23564050. [PubMed: 23564050]

31. Yeatman JD, Dougherty RF, Myall NJ, Wandell BA, Feldman HM. Tract Profiles of White Matter Properties: Automating Fiber-Tract Quantification. PLoS ONE. 2012; 7(11):e49790. [PubMed: 23166771]

32. Yeatman JD, Dougherty RF, Rykhlevskaia E, Sherbondy AJ, Deutsch GK, Wandell BA, et al. Anatomical properties of the arcuate fasciculus predict phonological and reading skills in children. Journal of Cognitive Neuroscience. 2011; 23(11):3304–17. PubMed PMID: 21568636. Pubmed Central PMCID: NIHMS332282 PMC3214008. [PubMed: 21568636]

33. De Santis S, Drakesmith M, Bells S, Assaf Y, Jones DK. Why diffusion tensor MRI does well only some of the time: variance and covariance of white matter tissue microstructure attributes in the living human brain. Neuroimage. 2014; 89:35–44. PubMed PMID: 24342225. Pubmed Central PMCID: PMC3988851. [PubMed: 24342225]

34. Feldman HM, Lee ES, Loe IM, Yeom KW, Grill-Spector K, Luna B. White matter microstructure on diffusion tensor imaging is associated with conventional magnetic resonance imaging findings and cognitive function in adolescents born preterm. Developmental Medicine & Child Neurology. 2012; 54(9):809–14. PubMed PMID: 22803787. [PubMed: 22803787]

35. Feldman HM, Lee ES, Yeatman JD, Yeom KW. Language and reading skills in school-aged children and adolescents born preterm are associated with white matter properties on diffusion

tensor imaging. Neuropsychologia. 2012; 50(14):3348–62. PubMed PMID: 23088817. Pubmed Central PMCID: NIHMS419970 [Available on 12/01/13] PMC3631607 [Available on 12/01/13]. [PubMed: 23088817]

36. Rohde GK, Barnett AS, Basser PJ, Marenco S, Pierpaoli C. Comprehensive approach for correction of motion and distortion in diffusion-weighted MRI. Magnetic Resonance in Medicine. 2004; 51(1):103–14. PubMed PMID: 14705050. [PubMed: 14705050]
37. Chang LC, Jones DK, Pierpaoli C. RESTORE: robust estimation of tensors by outlier rejection. Magnetic Resonance in Medicine. 2005; 53(5):1088–95. PubMed PMID: 15844157. [PubMed: 15844157]
38. Basser PJ, Pierpaoli C. Microstructural and physiological features of tissues elucidated by quantitative-diffusion-tensor MRI. Journal of Magnetic Resonance Series B. 1996; 111(3):209–19. PubMed PMID: 8661285. [PubMed: 8661285]
39. Mori, S.; Wakana, S.; van Zijl, PC.; Nagae-Poetscher, LM. MRI Atlas of Human White Matter. Elsevier; Amsterdam: 2005.
40. Conturo TE, Lori NF, Cull TS, Akbudak E, Snyder AZ, Shimony JS, et al. Tracking neuronal fiber pathways in the living human brain. Proceedings of the National Academy of Sciences of the United States of America. 1999; 96(18):10422–7. PubMed PMID: 10468624. Pubmed Central PMCID: PMC17904. [PubMed: 10468624]
41. Mori S, Crain BJ, Chacko VP, van Zijl PC. Three-dimensional tracking of axonal projections in the brain by magnetic resonance imaging. Annals of Neurology. 1999; 45(2):265–9. PubMed PMID: 9989633. [PubMed: 9989633]
42. Press, W.; Teukolsky, S.; Vetterling, W.; Flannery, B. Numerical Recipes in C++:The Art of Scientific Computing. Cambridge Univ Press; Cambridge, UK: 2002.
43. Dougherty RF, Ben-Shachar M, Deutsch GK, Hernandez A, Fox GR, Wandell BA. Temporal-callosal pathway diffusivity predicts phonological skills in children. Proceedings of the National Academy of Sciences of the United States of America. May 15; 2007 104(20):8556–61. PubMed PMID: 17483487. [PubMed: 17483487]
44. Granziera C, Schmahmann JD, Hadjikhani N, Meyer H, Meuli R, Wedeen V, et al. Diffusion spectrum imaging shows the structural basis of functional cerebellar circuits in the human cerebellum in vivo. PLoS ONE [Electronic Resource]. 2009; 4(4):e5101. PubMed PMID: 19340289. Pubmed Central PMCID: PMC2659746.
45. Ben-Yehudah G, Fiez JA. Impact of cerebellar lesions on reading and phonological processing. Annals of the New York Academy of Sciences. 2008; 1145:260–74. PubMed PMID: 19076402. [PubMed: 19076402]
46. Nichols TE, Holmes AP. Nonparametric permutation tests for functional neuroimaging: a primer with examples. Human Brain Mapping. 2002; 15(1):1–25. PubMed PMID: 11747097. [PubMed: 11747097]
47. Tuch DS, Reese TG, Wiegell MR, Makris N, Belliveau JW, Wedeen VJ. High angular resolution diffusion imaging reveals intravoxel white matter fiber heterogeneity. Magnetic Resonance in Medicine. 2002; 48(4):577–82. PubMed PMID: 12353272. [PubMed: 12353272]
48. Takahashi E, Hayashi E, JD S, Grant E. Development of cerebellar connectivity in human fetal brains revelaed by high angular resolution diffusion tractogrphy. Neuroimage. 2014; 96:326–33. Epub doi 10.1177/0883073809338067. [PubMed: 24650603]
49. Schmahmann JD, Caplan D. Cognition, emotion and the cerebellum. Brain. 2006; 129(Pt 2):290–2. PubMed PMID: 16434422. [PubMed: 16434422]
50. Tuch DS, Reese TG, Wiegell MR, Wedeen VJ. Diffusion MRI of complex neural architecture. Neuron. 2003; 40(5):885–95. PubMed PMID: 14659088. [PubMed: 14659088]
51. Tournier JD, Yeh CH, Calamante F, Cho KH, Connelly A, Lin CP. Resolving crossing fibres using constrained spherical deconvolution: validation using diffusion-weighted imaging phantom data. Neuroimage. 2008; 42(2):617–25. PubMed PMID: 18583153. [PubMed: 18583153]
52. Catani M, Jones DK, Daly E, Embiricos N, Deeley Q, Pugliese L, et al. Altered cerebellar feedback projections in Asperger syndrome. Neuroimage. 2008; 41(4):1184–91. PubMed PMID: 18495494. [PubMed: 18495494]

53. Riley JD, Franklin DL, Choi V, Kim RC, Binder DK, Cramer SC, et al. Altered white matter integrity in temporal lobe epilepsy: association with cognitive and clinical profiles. Epilepsia. 2010; 51(4):536–45. PubMed PMID: 20132296. Pubmed Central PMCID: NIHMS230341 PMC2929974. [PubMed: 20132296]

54. Travis KE, Leitner Y, Feldman HM, Ben-Shachar M. Cerebellar white matter pathways are associated with reading skills in children and adolescents. Human Brain Mapping. 2014 n/a n/a.

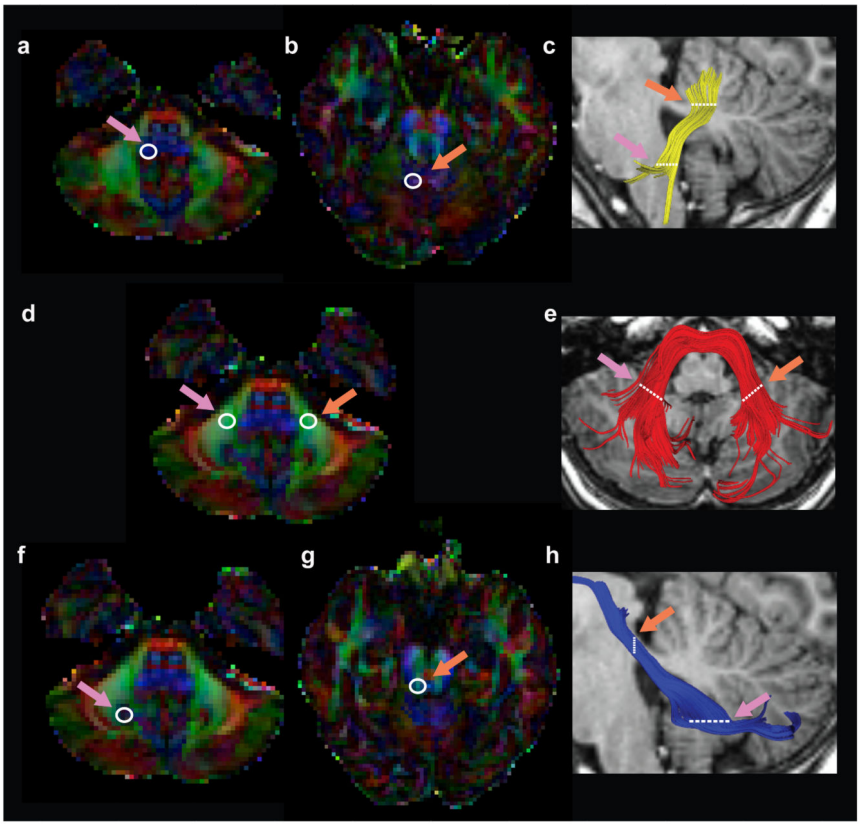

Figure 1.

Location of anatomical reference ROIs used for tractography. Left hand columns display axial dMRI red-green-blue (RGB) color maps used to identify the ICP (A,B), MCP (D) and SCP (F,G) tracts. Right hand column displays results of the tracking approach in a representative subject for the left ICP (C-yellow), MCP (E-red) and left SCP (H-blue). The two way point ROIs used to identify the ICP (A,B), MCP (D) SCP (F,G) are indicated by white circles. Only left hemisphere ROIs are displayed for the ICP and SCP. Single pink arrow refers to first ROI (ROI1, white circle) used to initiate tracking. Single orange arrow indicates second ROI (ROI2) used to constrain tracts and interest tracking initiated from ROI1. (ICP = inferior cerebellar peduncle; MCP = middle cerebellar peduncle; SCP = superior cerebellar peduncle. L = left; R = right).

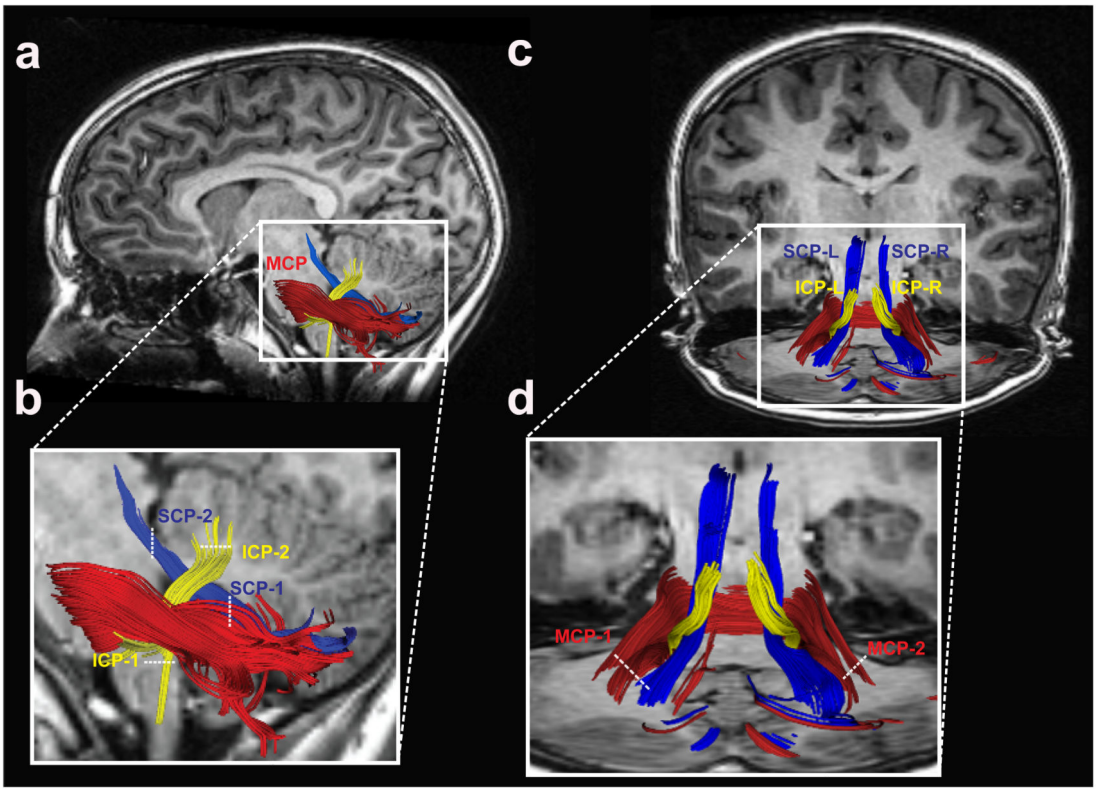

Figure 2.

Tractography of the cerebellar peduncles. Two-dimensional rendering of the inferior (yellow), middle (red) and superior (blue) cerebellar peduncles displayed on a left sagittal section of a representative subject (A-B). Coronal view of all cerebellar peduncles in the same representative subject (C-D). White dashed lines represent location of each of two ROIs used to define individual cerebellar tracts. (ICP = inferior cerebellar peduncle; MCP = middle cerebellar peduncle; SCP = superior cerebellar peduncle. L = left; R = right).

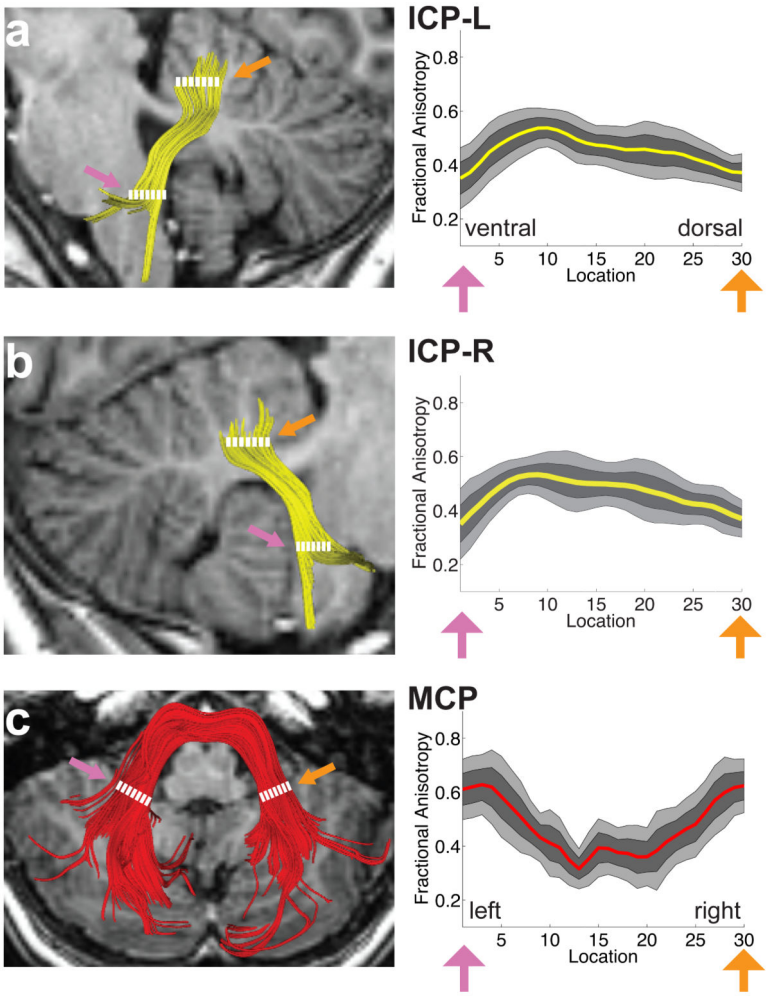

Figure 3.

FA tract profiles of the inferior and middle cerebellar peduncles in the sample of children and adolescents (N=19 ICP; N=18 MCP). Left hand column (A-C) shows renderings of 3 individual cerebellar tracts on sagittal (A,B) or axial (C) T1 images in the same representative subject shown in Figure 2. Right hand columns show FA tract profiles that are color-coded to match tract renderings in adjacent T1 images for the left (A) and right (B) ICP and MCP (C). FA values are plotted for 30 equidistant locations between two defining ROIs as indicated by dashed white lines. Location of ROIs correspond to pink and orange arrows in tract profiles. Boundaries of the 25th and 75th percentiles are indicated by dark gray shading. Boundaries of the 10th and 90th percentiles are indicated by light gray shading. (ICP = inferior cerebellar peduncle; MCP = middle cerebellar peduncle; L = left; R = right).

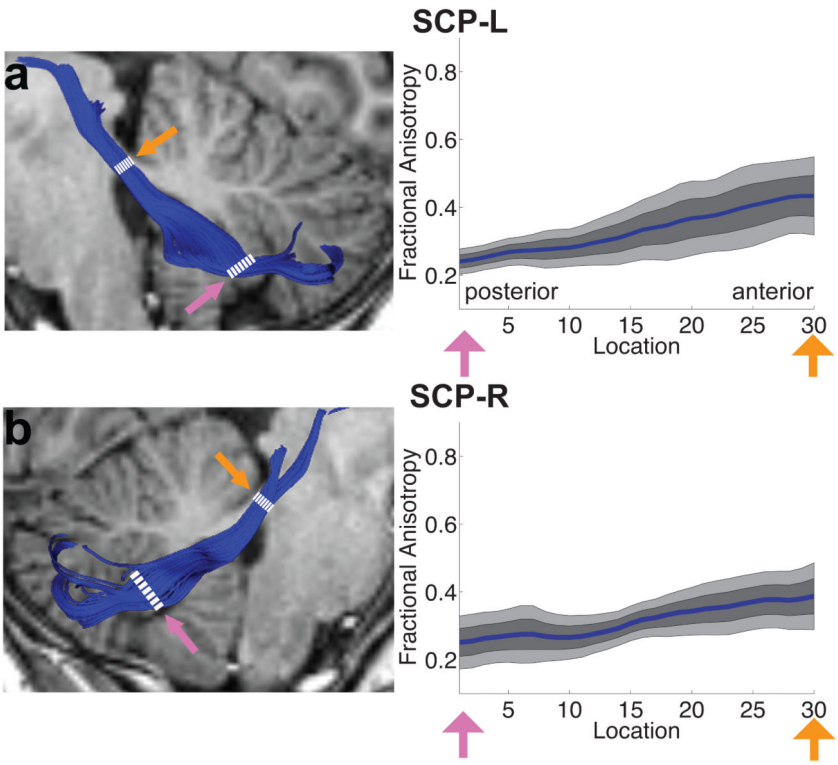

Figure 4.

FA tract profiles of superior cerebellar peduncles in the sample of children and adolescents (N=19). Left hand column (A,B) shows renderings of 2 individual cerebellar tracts on sagittal T1 images in the same representative subject shown in Figure 2. Right hand columns show FA tract profiles that are color-coded to match tract renderings in adjacent T1 images for the left (A) and right (B) SCP. FA values are plotted for 30 equidistant locations between two defining ROIs as indicated by dashed white lines. Locations of ROIs correspond to pink and orange arrows in tract profiles. Boundaries of the 25th and 75th percentiles are indicated by dark gray shading. Boundaries of the 10th and 90th percentiles are indicated by light gray shading. (SCP = superior cerebellar peduncle; L = left; R = right).

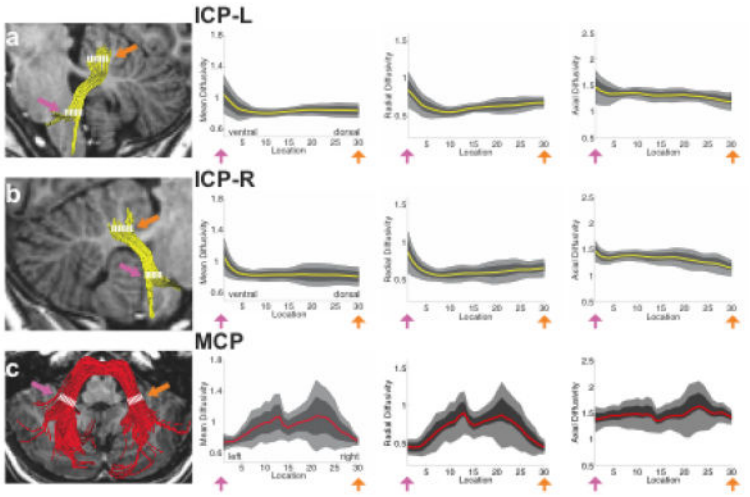

Figure 5.

Tract Mean Diffusivity (MD), Radial Diffusivity (RD) and Axial Diffusivity (AD) profiles of inferior, middle and superior cerebellar peduncles in the sample of children and adolescents. Columns show tract MD, RD and AD profiles that are color-coded to match tract renderings in T1 images presented in Figures 2-4. MD, RD and AD values are plotted for 30 equidistant locations between two defining ROIs. Locations of ROIs correspond to pink and orange arrows in tract profiles in Figures 2-4. Boundaries of the 25th and 75th percentiles are indicated by dark gray shading. Boundaries of the 10th and 90th percentiles are indicated by light gray shading. (ICP = inferior cerebellar peduncle; MCP = middle cerebellar peduncle; SCP = superior cerebellar peduncle; L = left; R = right).

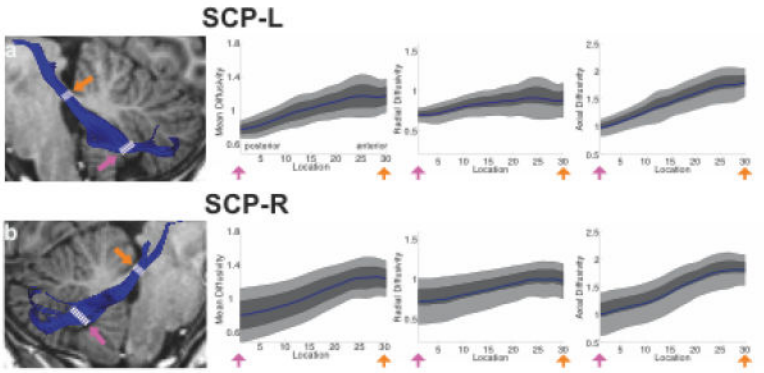

Figure 6.

Group and individual variance in Tract FA profiles. Group mean FA for the normative group is plotted for each tract for 3 locations corresponding to the average FA from nodes 1-10, 11-20, and 21-30 respectively (a-e). Error bars represent ±1 standard deviation of the normative group mean. (ICP = inferior cerebellar peduncle; MCP = middle cerebellar peduncle; SCP = superior cerebellar peduncle; L = left; R = right).

Table 1

Variance in Tract Fractional Anisotropy profiles for the normative group

	Subdivision 1 (nodes 1-10)			Subdivision 2 (nodes 11-20)			Subdivision 3 (nodes 21-30)		
Tract	**Mean**	**(std)**	**CV**	**Mean**	**(std)**	**CV**	**Mean**	**(std)**	**CV**
ICP-L	0.47	(0.07)	14.15	0.48	(0.05)	11.43	0.42	(0.05)	13.01
ICP-R	0.47	(0.06)	13.00	0.50	(0.06)	12.96	0.42	(0.06)	13.69
MCP	0.54	(0.06)	11.71	0.37	(0.06)	15.46	0.51	(0.06)	12.89
SCP-L	0.26	(0.03)	10.05	0.33	(0.06)	19.30	0.41	(0.08)	20.47
SCP-R	0.27	(0.05)	19.40	0.31	(0.04)	12.87	0.37	(0.06)	15.82

CV = coefficient of variance; std = standard deviation; ICP = Inferior Cerebellar Peduncle, MCP = Middle Cerebellar Peduncle, SCP = Superior Cerebellar Peduncle; L= left; R= right

Table 2

Variance in Tract Mean Diffusivity profiles for the normative group

	Subdivision 1 (nodes 1-10)			Subdivision 2 (nodes 11-20)			Subdivision 3 (nodes 21-30)		
Tract	**Mean**	**(std)**	**CV**	**Mean**	**(std)**	**CV**	**Mean**	**(std)**	**CV**
ICP-L	0.87	(0.09)	9.98	0.83	(0.02)	35.88	0.84	(0.02)	42.26
ICP-R	0.86	(0.09)	10.08	0.83	(0.03)	29.30	0.83	(0.03)	30.89
MCP	0.86	(0.12)	7.28	1.01	(0.11)	8.88	0.94	(0.16)	5.83
SCP-L	0.86	(0.06)	14.20	1.05	(0.08)	13.84	1.17	(0.06)	20.46
SCP-R	0.87	(0.05)	19.40	1.06	(0.08)	12.65	1.24	(0.07)	18.13

CV = coefficient of variance; std = standard deviation; ICP = Inferior Cerebellar Peduncle, MCP = Middle Cerebellar Peduncle, SCP = Superior Cerebellar Peduncle; L= left; R= right